Available online at www.sciencedirect.com

ScienceDirect

Carbon 45 (2007) 1786–1794

CARBON

www.elsevier.com/locate/carbon

The effect of temperature on nanoparticle clustering

Steven L. Fiedler, Sergei Izvekov [1], Angela Violi *

Department of Mechanical Engineering, University of Michigan, Ann Arbor, MI 48109-2125, United States

Received 12 February 2007; accepted 2 May 2007
Available online 13 May 2007

Abstract

A multiscale computational approach was applied to study the evolution of soot formation in an ethylene flame environment, from small polycyclic aromatic hydrocarbons of less than 10 atoms, to nano-sized organic carbon (NOC) clusters of diameters up to 15 nm. As this evolution covers sizable breadth in time and length scales, the application of a sequence of complementary computational approaches was employed. To model NOC particle aggregation, the coarse grain method allowed for molecular dynamics simulation of over 13,000 nanoparticles (10^6 atoms), for hundreds of nanoseconds. Notable growth in both the number and size of particles was observed when temperature was dropped from 1800 to 300 K. A test of input sensitivity determined little noticeable effect upon inclusion of electrostatic interactions of atomic-centered partial charges. These results provide insights on the influence of temperature on nanoparticle aggregation in flames. This could also assist in the analysis of experimental measurements of methods which allow for sample cooling in the period from extraction to detection.

1. Introduction

Elucidating the earliest steps in soot formation is currently an increasingly active field of research, with recent advances in experimental methods enabling a nanoscopic view of some of the smallest structures and dynamics within flame environments. The processes involved in the formation of particles exhibit a wide range of time scale, spanning pico- or nanoseconds for intramolecular processes to milliseconds for intermolecular reactions. Particle formation begins with the formation of polycyclic aromatics (PAH) from individual fuel components, followed by particle inception and their subsequent coagulation and agglomeration leading to primary particles (50 nm in diameter). During these processes, the length scale also undergoes significant changes going from a few Angstroms for small PAH to hundreds of nanometers for particle aggregates.

This paper reports on a multiscale coarse-graining simulation approach for bridging the time and length scales in the growth of the carbon nanoclusters. The specific goals are to: (1) study the particle coagulation in the range 3–10 nm occurring in an ethylene flame using multiscale atomistic methods and (2) assess the effect of temperature on particle coagulation. The latter could provide experimental guidance; the very act of many measurements themselves introduces perturbations to the system, or can create a non-representative sample prior to analysis. This study will focus on one such phenomenon, the process of nanoparticle aggregation, their binding as function of temperature, which could occur in transit when molecular entities are cooled in the process of being removed from flame environments. Standard experimental techniques including transmission electron microscopy (TEM) and scanning mobility particle sizer (SMPS) have been questioned in this regard [1]. To this end, a set of available computational tools to model the temperature dependence on nanoparticle cluster growth, i.e., "nano-condensation" will be applied.

---

* Corresponding author. Fax: +1 734 647 9679.
E-mail address: avioli@umich.edu (A. Violi).

[1] Present address: Department of Chemistry, University of Utah, Salt Lake City, UH 84112-0850, United States.

0008-6223/$ - see front matter © 2007 Elsevier Ltd. All rights reserved.
doi:10.1016/j.carbon.2007.05.001

2. Methodology

To study the sequence of formation events in high temperature regime, i.e., particle structures and dynamics, the following suite of programs were employed. Growth of incipient particles from small PAH was simulated using the Atomistic Model Particle Inception (AMPI) program [2–4], which is designed to couple the kinetic Monte Carlo and molecular dynamics (MD) techniques to bridge the timescales between and during reaction events. Properties of nanoparticles generated with the AMPI code have shown to reproduce data, such as H/C and aspect ratios, comparable with experiments [3–5]. The AMPI code is used in this work to produce an ensemble of nanoparticles at a specific location in an ethylene premixed flame.

The intermolecular scale between the nanoparticles is described using a coarse-grained molecular dynamics approach. To observe a statistically significant number of coagulation events, a large particle ensemble (10^4) has been shown to be effective [6–8]. This corresponds to running force field-based MD of over millions of atoms for simulation times on the order of hundreds of nanoseconds, which cannot be achieved in a reasonable research time frame using the current processing power available. One option is to depart from an all atom calculation, and in essence lower the resolution. The approach used in this proposal is based on the multiscale coarse-graining methodology [6–10] in which a detailed atomistic model is transformed into a lower resolution model via a systematic and thermodynamically consistent procedure in which pre-selected atomic groups are collated into new coarse-grained quasi-molecular units. Thus, a nanoparticle of ~450 atoms can be represented as a single particle, i.e., coarse-grained to one site. Assigning three sites per molecule, however, will allow for consideration of anisotropy.

The most critical and challenging stage in the implementation of these approaches is the determination of the intermolecular forces to describe the interactions between the new effective coarse grain (CG) sites. In this paper, the force matching (FM) algorithm was employed to this end [6,9]. The details of FM algorithm can be found in the references listed, with the basic premise being that effective CG potentials can be uniquely and directly extracted from reference atomistic dynamics. The multiscale computational approach presented reflects the fact that an application of the FM procedure to the CG images from underlying atomistic trajectory/force data should produce the effective interaction between CG structural units as it seen in the atomistic dynamics.

The MD program DL_POLY 2.16 [11], was used in a parallel capacity to generate all atom reference trajectories for a system containing a limited number of NOC particles replicated from the AMPI produced structures described above. The FM routines then calculated the non-bonded interactions, and MD simulations were run for large ensembles containing ~10^4 coarse-grained nanoparticles, equivalent to millions of atoms.

3. Results and discussion

Keeping in mind that the overarching goal of this study is to investigate the interactions between carbonaceous particles of different morphologies and chemical compositions, this systematic multi-scaling study was begun at an atomistic-level of resolution. Fig. 1 shows the structures of four nanoparticles produced at a height of 6 mm above the burner of a premixed ethylene flame (C/O = 0.77) at atmospheric pressure using the AMPI code. This flame has been well experimentally characterized using different techniques, including UV–vis light absorption, laser-excited fluorescence, laser-induced incandescence, light scattering [12], and differential mobility analysis [13]. The gas-phase environments of the flame at different distances from the burner were obtained from a previously developed kinetic mechanism [14,15] and the resultant number of concentration of species and temperature were used as input to the AMPI code. The accuracy of the mechanism in reproducing species concentration has been previously reported [16–18]. Results from the atomistic code were averaged in terms of number of aromatic rings and functional groups and the structures reported in Fig. 1 represent particle averages.

The criterion that the particle should exceed a threshold mass to support dispersion interactions was used to determine the size of the representative NOC particles. Minimal mass estimates have been calculated to range from 1600 and 3000 a.m.u., depending on the source [19]. Using this as a guide of a lower limit, for this study the average size grown was around 450 total atoms, 30 Å in diameter, and corresponding of mass of 3120 a.m.u. These particles possess flat leaf-like aromatic planes, and a general lack of overall curvature, which have been noted as distinguishing characteristics of the ethylene nanoparticles [2].

Atomistic molecular dynamics simulations were employed to both serve as a computational template on which to base the coarse-graining step of the multiscale computational paradigm as well as to provide a comparison for properties of the "lower resolution" CG system. To address the latter, molecular dynamics simulations of two nanoparticles of type I (Fig. 1) were carried out to determine the bimolecular binding based on atomic interactions. The particles with rigid intramolecular bonds, and C–C, C–H, and H–H van der Waals' force field parameters taken from the aromatic CHARMM [20] parameters,

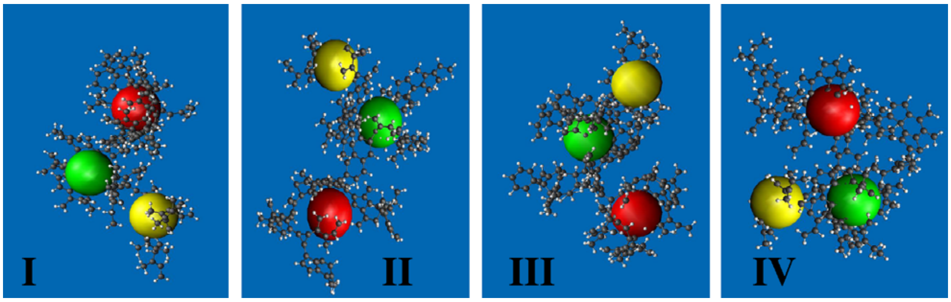

Fig. 1. NOC structures generated in an ethylene flame as calculated with AMPI represented by the smaller grey and white spheres for carbon and hydrogen, respectively. The superimposed yellow, green, and red spheres, represent the three CG sites on each molecule. Note as each sphere represents a different atomic configuration, the CG intermolecular interactions, i.e., between each CG site, are unique. (For interpretation of the references to color in this figure legend, the reader is referred to the web version of this article.)

CA–CA, CA–HP, and HP–HP, respectively, were initially separated by 70 Å and given 100 K of kinetic energy.

Fig. 2 illustrates the change in configurational energy of the system. The results show the complexity of the binding due to the sampling of many local minima on the global potential energy surface.

Clearly, the bimolecular potential should not be expected to be adequately described by a smooth analytical, Lennard–Jones type function. In fact, due to the intricate NOC particle morphologies, one could imagine a great deal of jostling to be necessary for the two particles to locate the global minimum on the potential energy surface. Fortunately, a free energy pair "potential" falls out of the CG/FM methodology naturally, which by definition contains angular averaging.

To create a representative ethylene flame environment, a system was constructed with 64 NOC particles of four types (Fig. 1, I–IV), 16 each and the calculation was run for 10 ns within the canonical ensemble using a Berendsen thermostat [21] with a 0.1 ps relaxation constant, at 1100 K, using a 0.02 ps time-step, with a velocity Verlet integrator, and periodic boundary conditions. The system was thermalized and an accurate sampling of the dynamical configurations of the atomistic trajectory was obtained. This step is required to build a reference data set for the force matching process. Fig. 3 (black curve) shows the radial distribution function (RDF) profiles for different pair of particles. The convergence in the noise of the nanoparticle RDF and force ensure proper sampling in configuration space.

The individual NOC particles produced by the AMPI code were partitioned into three sites. Fig. 1 shows the three coarse-grained sites (yellow, green and red) for each of the nanoparticles considered in this study. Assignment of the three CG sites for each NOC particle was performed by a combination of inspection of the structure and chemical intuition, e.g., double bonds were allowed to remain intact, contiguous static regions of the structure were contained within one CG, etc.

In order to assess the accuracy of the coarse-graining method, a preliminary comparison was taken between the results obtained using the atomistic approach and the dynamics of a system of 64 CG particles (3-CG sites). The GC system was simulated under the same conditions as the atomistic MD simulation, and the resultant RDFs for the CG system were compared with the atomistic results (Fig. 3). Significant deviation between RDFs based on atomistic vs. CG trajectories would be an indication of inadequate sampling within the atomistic reference trajectory. The average binding of the three-site potentials was determined to be around 26.9 meV.

As observed previously [6,7], the degree of intermolecular binding differs by orders of magnitude between the atomistic and CG potentials. The difference lies in the fact that the CG potential represents a free energy potential including both the influence of temperature, as well as configurational averaging. For example, Fig. 2 clearly demonstrates the presence of multiple narrow local minima which may not be readily accessible and thus not contribute greatly to a intermolecular free energy potential at high temperatures. It should be noted, however, that 97% of the three-site CG potentials were bound, and binding is certainly required for coagulation.

To assess the importance of electrostatic interactions on the binding of nanoparticles, atomic partial charges for the nanoparticles generated with the AMPI code were

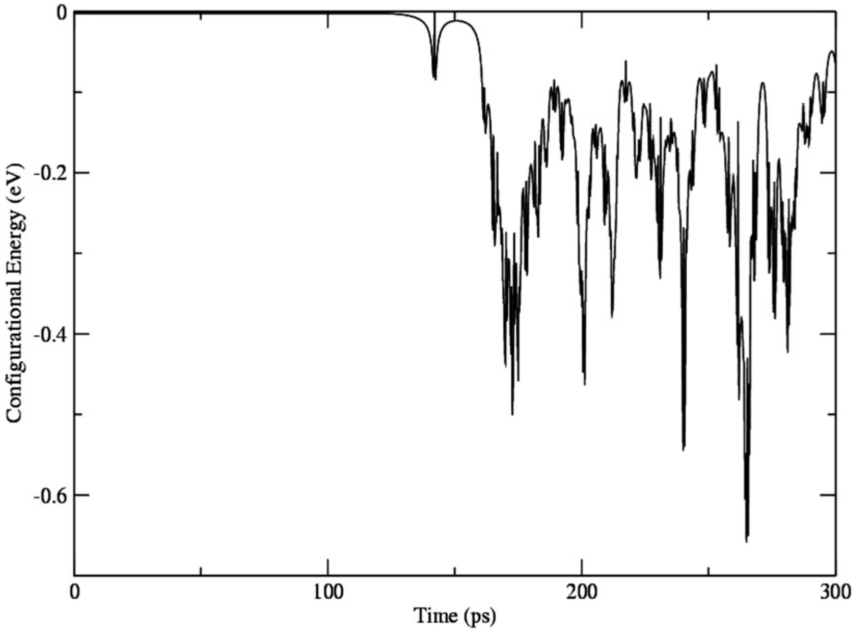

Fig. 2. MD trajectory of two NOC particles (I from Fig. 1) revealing the complex bimolecular potential energy surface. The two molecules were initially separated by 70 Å, and run within the microcanonical ensemble.

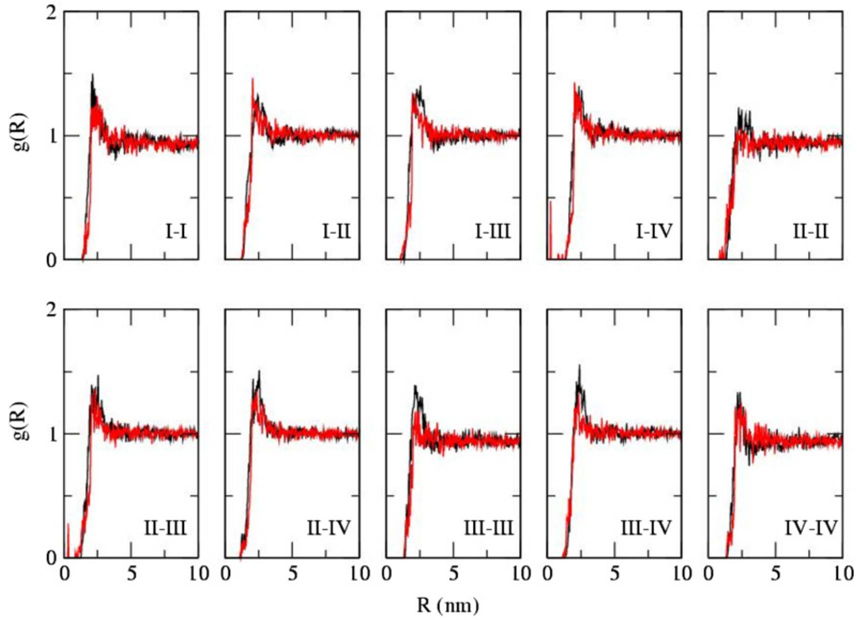

Fig. 3. Representative radial distribution function comparison of atomistic (black) vs. CG NOC particles (red). Roman numerials refer to particle types depicted in Fig. 1. (For interpretation of the references to color in this figure legend, the reader is referred to the web version of this article.)

calculated as fitted to the electrostatic potential with the electrostatic potential fitting (EPF) method within the Gaussian'03 package [22]. The EPF method was selected as it, by design, assigns partial charges based on van der Waals interactions, which are the relevant quantities of this study. Additionally, it has been shown that EPF partial charges of PAH, NOC precursors, attained more physical reasonable quantities, i.e., positive partial charges on hydrogen, and better transferability of charges between similar species, when compared to the Mulliken analysis [23]. The electronic structures of the NOC particles were calculated by density function theory using the B3LYP functional [24], and a 6-31G(d) basis. Partial charges were then included in the following MD calculations. A system of 32 nanoparticles of two types (Fig. 1a and b), 16 each, in box with a length of 1.09 nm was constructed. The Smoothed Particle Mesh Ewald (SPME) method with an automatic optimization parameter of 1×10^{-5}, was used to determine the electrostatic contribution to the forces. To benchmark, a parallel (two processor), DL_POLY 2.16, MD calculation on a dual processor 1.4 GHz AMD Opteron, 240, with 2 GB of memory per cpu, proceeded at a rate of 51 h/ns with electrostatic inclusion, and 18 h/ns without. The resultant CG potentials between nanoparticles of types I and I, I and II, and II and II are overlaid with their respective non-electrostatic counterpart in Fig. 4. The computed potentials appear to possess some deviation in form from those calculated without consideration of the partial charge electrostatic interactions, however, the benefit for their inclusion should be weighed against the additional computational expense.

The overall interaction potential is a function of the particle sizes and the Hamaker constant A, where $A = \pi^2\rho^2C$, ρ is the particle density and C is the London dispersion force coefficient, that is proportional to particle polarizability and ionization potential [25]. For direct experimental comparison, the value of the Hamaker constant, can be determined by the Hamaker summation potential between two spheres, which reduces in our case to: $A = 24\Phi_0$, where Φ_0 is the binding energy. For the representative NOC particles in this study, the average value of A is calculated to be 0.65 eV. This value falls between that of hydrocarbons, 0.3 eV [25], and graphite 3 eV [26] indicating a significant degree of aromatization of the structures.

A related quantity, the sticking probability, γ, is the probability of attachment upon collision, and is based on the fraction of particles having kinetic energy less than the intermolecular potential. Given a Maxwell–Boltzmann kinetic energy distribution, γ can be defined as a function of temperature, T, to be,

$$\gamma(T) = 1 - \frac{1 + D_e/kT}{e^{D_e/kT}}$$

where, k is the Boltzmann's constant, and D_e is the average three-site potential depth (26.9 meV). This corresponds to a resultant sticking probability value of 0.0134 for 1800 K. This number compares reasonably well with the experimental value obtained through spectroscopic characterization of this flame [12].

To obtain a representative configuration of $\sim 10^4$ CG particles, the final configuration from the 10 ns atomistic trajectory was replicated $6 \times 6 \times 6$ times to form a supercell containing a total of 13,824 particles. As the focus of this study was on cluster evolution as opposed to formation, and the excessive simulation time required for the latter, the initial configuration of the CG simulation was

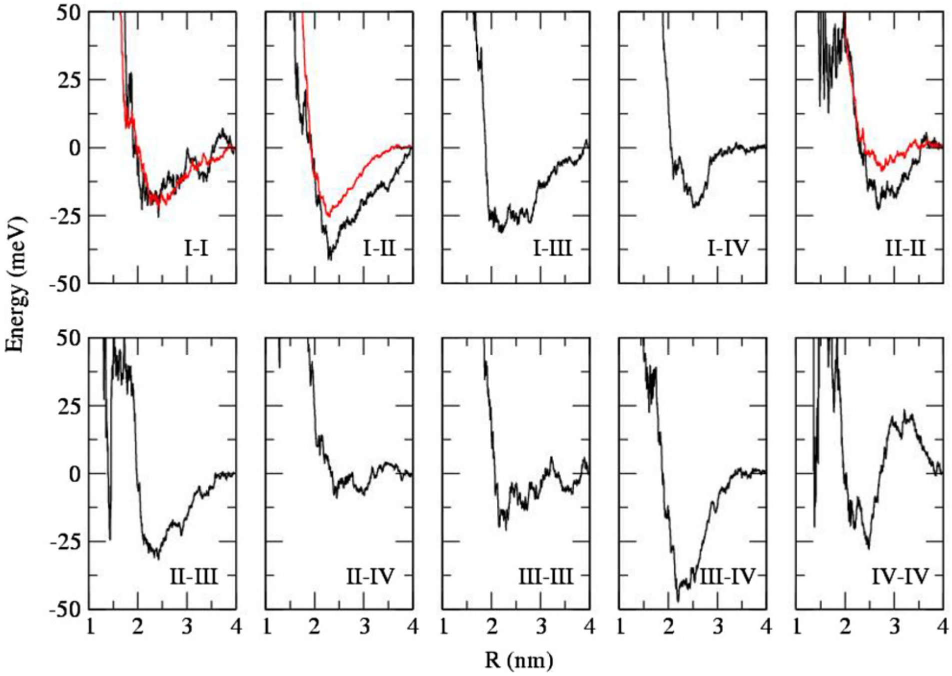

Fig. 4. CG pair potentials between NOC particles (black lines). Red lines are the corresponding CG pair potentials for 32 NOC particle of two types (I and II) system calculated with inclusion of electrostatic interactions. Roman numerials refer to particle types depicted in Fig. 1. (For interpretation of the references to color in this figure legend, the reader is referred to the web version of this article.)

"seeded" with small pre-optimized structures (1–20 nm) and the system was studied at 1800 K. This procedure has been proven to adequately reproduce the properties of the system [6,7,27]. Fig. 5 displays a representative configuration containing incipient clusters, color coded according to size. A nearest neighbor cutoff of 3 nm was selected as the cutoff criterion for cluster inclusion.

A histogram of cluster sizes at various times in the trajectory is shown in Fig. 6. As the simulation progresses, many of the particles on the seed clusters began to evaporate, and after 25 ns the size distribution reached convergence since after 75 ns the curve does not change.

The results show a unimodal size distribution spreading from 3 to 8 nm. Experimental data reported for this flame from spectral analysis [12], differential mobility analyzer, and atomic force microscopy [13] shows a particle size distribution around 3–4 nm that agrees quite well with the computational results reported in this paper.

3.1. Effect of temperature

The second objective of this paper is to address the influence of temperature on particle size distribution. This correlation has been experimentally observed to significantly alter even qualitative features of the PSD profiles [29]. Consequently, it raises concern for analysis of ex situ PSD measurements that inherently allow for the sample to cool prior to evaluation. Specifically, the resultant PSD in this case may correspond to a non-equilibrium particle distribution, i.e., that of the ensemble subjected to a negative temperature gradient. Temperature directly regulates particle

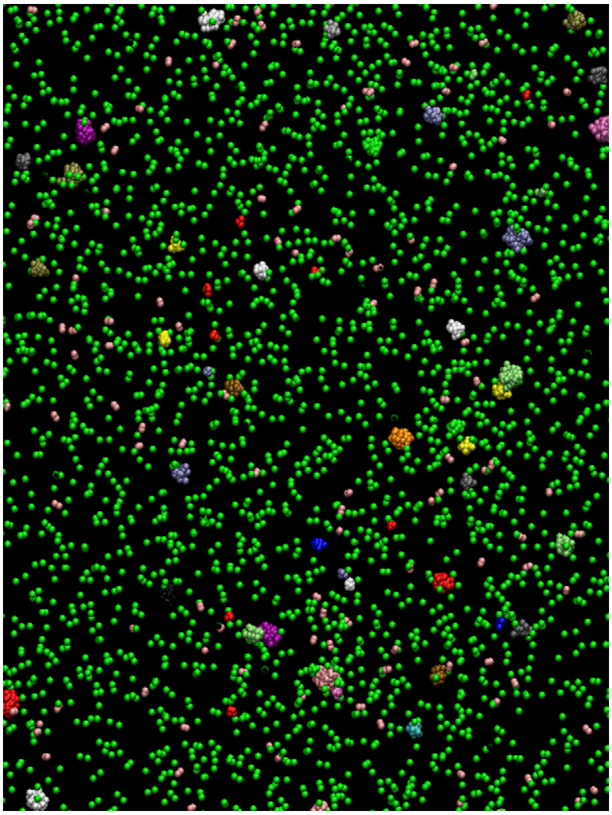

Fig. 5. Snapshot of a CG-MD trajectory. Each green sphere represents a three-site CG particle. Particle clusters are colored according to their size. (For interpretation of the references to color in this figure legend, the reader is referred to the web version of this article.)

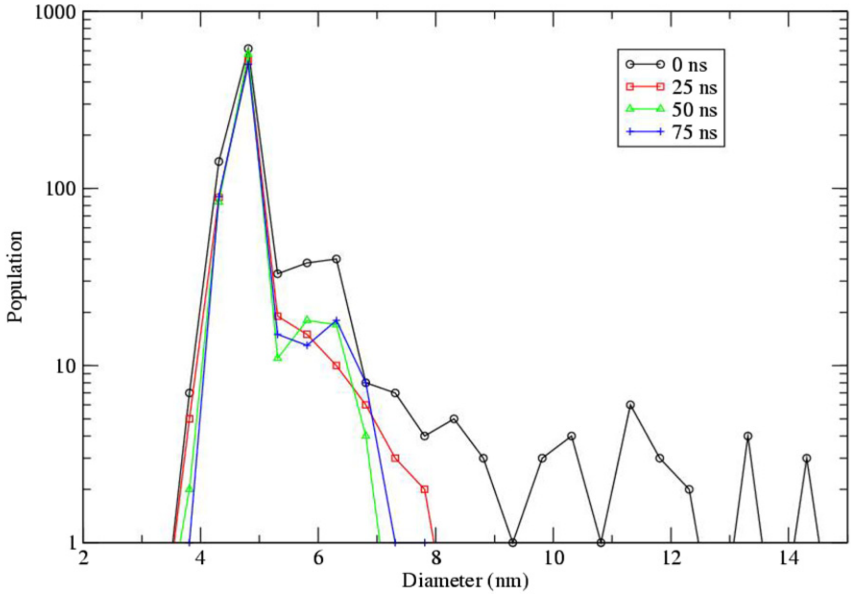

Fig. 6. Histogram of NOC particle cluster sizes at 1800 K at: 0 ns (○), 25 ns (□), 50 ns (△) and 75 ns (+).

kinetic energies and thus the coagulation efficiency. To model this scenario, the final configuration from the equilibrated 1800 K trajectory served as input for two new trajectories which brought the temperature system down to 500 K, and 300 K. Fig. 7 shows two snapshots from the simulations of 13,960 nanoparticles at 1800 K and 300 K. The figure clearly illustrates the formation of bigger agglomerates at low temperature.

A more quantitative measure of the effect of temperature on cluster formation is shown in Fig. 8a and b, which displays a histogram of particle number per cluster (Fig. 8a) and the particle cluster diameters (Fig. 8b) from equilibrated coarse-grained MD simulations at 1800, 500, and 300 K. As temperature decreases, the cluster size distribution spreads reaching sizes of almost 20 nm. A comparison of the particle size distribution functions (PSD) at the three temperatures reveal an initial gain in the population for all cluster sizes, followed by secondary coagulation events, as suggested by growth of large clusters (diameter > 4 nm) with the concurrent decline in the smaller cluster population.

The thermal energies of the nanoparticles at 300 K and at 1800 K are 26 and 155 meV, respectively. Coagulation of two particles occurs after collision if the kinetic energy of the particles is lower than their interaction potential. In particular, the depth of the potential well D_e is low respect to the gas kinetic energy (kT) at flame temperatures. It means that at 1800 K, most colliding particles have enough

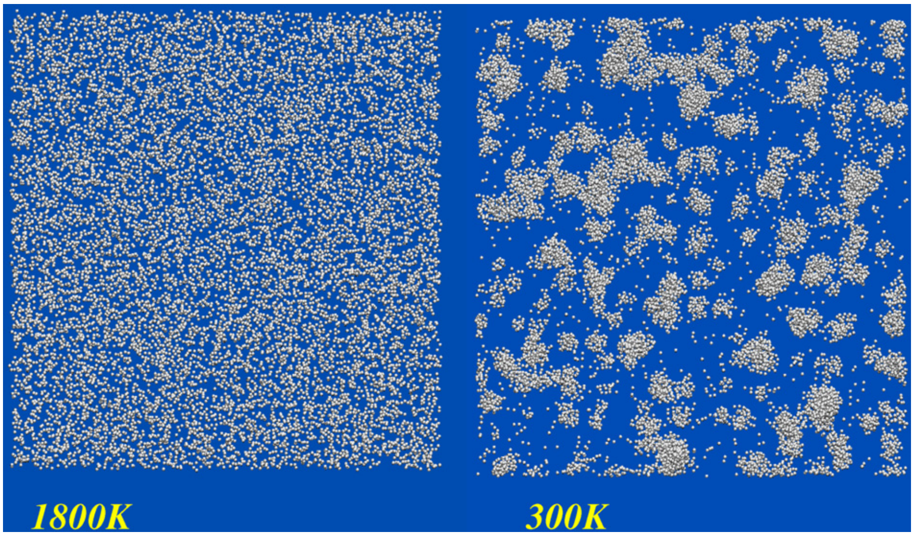

Fig. 7. Snapshot of 13,960 nanoparticles after equilibration at 1800 K and at 300 K.

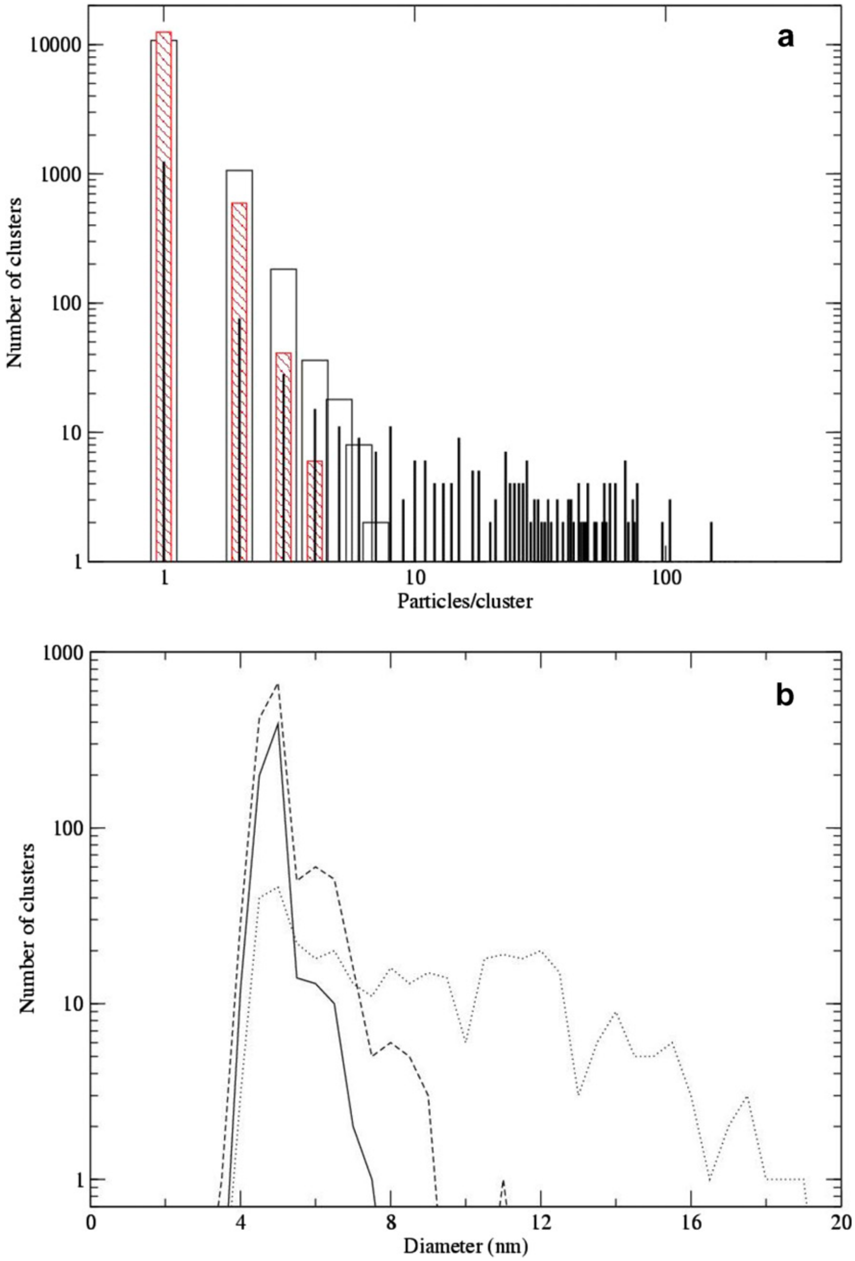

Fig. 8. Histogram of (a) particle number per cluster from equilibrated CG-MD trajectories at 1800 K (open rectangles), and after a subsequent temperature drop to (A) 500 K (striped rectangles) and (B) 300 K (sticks) and (b) of NOC particle cluster diameters from equilibrated CG-MD trajectories at 1800 K (solid line), and after a subsequent temperature drop to (A) 500 K (dashed line) and (B) 300 K (dotted line).

energy to escape from the potential well and hence to remain uncoagulated. Conversely, at lower temperatures the kinetic energy is reduced and the fraction of particles with kinetic energy less than the potential depth increases resulting in an increased sticking probability, e.g., rising from 0.0134 at 1800 K, to 0.279 at 300 K. At high temperatures, the kinetic energy of the relative motion of the nanoparticles exceeds the depth of the potential minimum and the time spent in the region of the interaction potential is also reduced by a factor of $(T_{\mathrm{low}}/T_{\mathrm{high}})^{1/2}$.

Particle size distributions for an ethylene flame (C_2H_4/O_2/Ar, $\Phi = 2.07$) similar to the one presented here have been obtained by SMPS measurements [28]. Bimodal distributions, were observed consisting of a dip at a particle diameter of 5 nm, which was attributed to an underlying competition between nucleation and coagulation [29]. Subsequently, the same authors reported SMPS measurements of a slightly richer flame (C_2H_4/O_2/Ar, $\Phi = 2.5$) and identified a bimodality with the dip at around 15 nm. Since this flame has a temperature profile ($T_{\mathrm{peak}} = \sim 1500$ K) much lower than the previous flame ($T_{\mathrm{peak}} = \sim 1750$ K) it is plausible that this could cause the formation of larger clusters.

Finally, these results might address the discrepancy commonly seen in the PSD determined by different techniques, such as SMPS and TEM. Zhao et al. [1] have recently reported a comparative study of nanoparticles by SMPS and TEM for the ethylene flame mentioned above ($\Phi = 2.5$) showing notable disagreement between the two techniques' sizes. In particular, TEM measurements did not detect particles <10 nm. The cause could be due to the different temperatures between the flame and the grid. Upon deposition on a TEM grid, nanoparticles will undergo a cooling process and as the computations showed, this will cause their clustering spreading the size distribution function towards higher values of the cluster diameter.

4. Conclusions

This work contributes to the understanding of nanoparticle formation in flames. Specifically, an inverse correlation is clearly demonstrated between temperature, i.e. kinetic energy, of a nanoparticle ensemble and the degree of aggregation. This holds particular significance for experimental analysis of particle size distributions, as current methods often inherently allow for a period of cooling prior to measurement. In this study, the growth of nanoparticles generated in an ethylene flame environment were simulated to sizes up to 15 nm in length, based solely on atomic interactions. To achieve simulation of over 13,000 particles (10^6 atoms) for hundreds of nanoseconds, the coarse grain and force matching methods were employed. The resultant intermolecular interaction potential depths were reported and compared to predicted literature values. Finally, a temperature dependence on particle aggregation was demonstrated, with particle size distributions calculated at intervals throughout the trajectories.

Acknowledgements

This research is funded by the US Air Force Scientific Office for Research (Grant No. FA9550-06-1-0376) and by National Science Foundation (Grant CTS 0553764). The authors wish to thank Prof. H. Houston Miller at The George Washington University for the insightful discussion on the electrostatic interactions on the binding of nanoparticles.

References

[1] Zhao B, Uchikawa K, Wang H. A comparative study of nanoparticles in premixed flames by scanning mobility particle sizer, small angle neutro scattering, and transmission electron microscopy. Proc Combust Inst 2007;31:851–60.

[2] Violi A. Modeling of soot particle inception in aromatic and aliphatic premixed flames. Combust Flame 2004;139(4):279–87.

[3] Violi A, Sarofim AF, Voth GA. Kinetic Monte Carlo molecular dynamics approach to model soot inception. Combust Sci Technol 2004;176(5–6):991–1005.

[4] Violi A, Venkatnathan A. Combustion-generated nanoparticles produced in a benzene flame: a multiscale approach. J Chem Phys 2006;125:054302.

[5] Violi A, Voth GA, Sarofim AF. The relative roles of acetylene and aromatic precursors during soot particle inception. Proc Combust Inst 2005;30:1343–51.

[6] Izvekov S, Violi A, Voth GA. Systematic coarse-graining of nanoparticle interactions in molecular dynamics simulation. J Phys Chem B 2005;109(36):17019–24.

[7] Izvekov S, Violi A. A coarse-grained molecular dynamics study of carbon nanoparticle aggregation. J Chem Theor Comput 2006;2(3):504–12.

[8] Violi A, Izvekov S. Soot primary particle formation from multiscale coarse-grained molecular dynamics simulation. Proc Combust Inst 2007:529–37.

[9] Izvekov S, Parrinello M, Burnham CJ, Voth GA. Effective force fields for condensed phase systems from ab initio molecular dynamics simulation: a new method for force-matching. J Chem Phys 2004;120(23):10896–913.

[10] Violi A, Voth GA. A multi-scale computational approach for nanoparticle growth in combustion environments. In: Proceedings of the high performance computing and communications; 2005. p. 938–47.

[11] Smith W, Forester TR. DL_POLY_2.0: a general-purpose parallel molecular dynamics simulation package. J Mol Graphics 1996;14(3): 136–141.

[12] Minutolo P, Gambi G, D'Alessio A, Carlucci S. Spectroscopic characterisation of carbonaceous nanoparticles in premixed flames. Atmos Environ 1999;33(17):2725–32.

[13] Sgro LA, Basile G, Barone AC, D'Anna A, Minutolo P, Borghese A, et al. Detection of combustion formed nanoparticles. Chemosphere 2003;51(10):1079–90.

[14] Violi A, D'Anna A, D'Alessio A. Modeling of particulate formation in combustion and pyrolysis. Chem Eng Sci 1999;54(15–16):3433–42.

[15] D'Anna A, Violi A. Detailed modeling of the molecular growth process in aromatic and aliphatic premixed flames. Energy Fuel 2005;19(1):79–86.

[16] D'Anna A, Violi A, D'Alessio A, Sarofim AF. A reaction pathway for nanoparticle formation in rich premixed flames. Combust Flame 2001;127(1–2):1995–2003.

[17] D'Anna A, Violi A, D'Alessio A. Modeling the rich combustion of aliphatic hydrocarbons. Combust Flame 2000;121(3):418–29.

[18] D'Anna A, Violi A. A kinetic model for the formation of aromatic hydrocarbons in premixed laminar flames. In: Burgess AR, Dryer FL, editors. Proceedings of the 27th symposium; 1998. p. 425–33.

[19] Bockhorn H, editor. General disscussion, soot formation in combustion. Heidelberg: Springer-Verlag; 1994. p. 108.

[20] Brooks BR, Bruccoleri RE, Olafson BD, States DJ, Swaminathan S, Karplus M. Charmm – a program for macromolecular energy, minimization, and dynamics calculations. J Comput Chem 1983;4(2):187–217.

[21] Berendsen HJC, Postma JPM, Vangunsteren WF, Dinola A, Haak JR. Molecular-dynamics with coupling to an external bath. J Chem Phys 1984;81(8):3684–90.

[22] Frisch MJ, Trucks GW, Schlegel HB, Scuseria GE, Robb MA, Cheeseman JR, et al. Gaussian'03. Pittsburgh, PA: Gaussian Inc.; 2003.

[23] Rapacioli M, Calvo F, Spiegelman F, Joblin C, Wales DJ. Stacked clusters of polycyclic aromatic hydrocarbon molecules. J Phys Chem A 2005;109(11):2487–97.

[24] Becke AD. Density-functional thermochemistry. 3. The role of exact exchange. J Chem Phys 1993;98(7):5648–52.

[25] Israelachvili JN. Intermolecular and surface forces. San Diego: Academic Press; 1992.

[26] D'Alessio A, Barone AC, Cau R, D'Anna A, Minutolo P. Surface deposition and coagulation efficiency of combustion generated nanoparticles in the size range from 1 to 10 nm. Proc Combust Inst 2005;30:2595–603.

[27] Violi A, Izvekov S. Soot primary particle formation from multiscale coarse-grained molecular dynamics simulation. Proc Combust Inst 2007;31:529–37.

[28] Zhao B, Yang ZW, Johnston MV, Wang H, Wexler AS, Balthasar M, et al. Measurement and numerical simulation of soot particle size distribution functions in a laminar premixed ethylene–oxygen–argon flame. Combust Flame 2003;133(1–2):173–88.

[29] Zhao B, Yang Z, Li Z, Johnston MV, Wang H. Particle size distribution function of incipient soot in laminar premixed ethylene flames: effect of flame temperature. Proc Combust Inst 2005;30: 1441–8.